Self-consistent Green-function method for the calculation of electronic properties of localized defects at surfaces and in the bulk

1992 J. Phys.: Condens. Matter 4 2831

(http://iopscience.iop.org/0953-8984/4/11/011)

J. Phys.: Condens. Matter 4 (1992) 2831–2844. Printed in the UK

Self-consistent Green-function method for the calculation of electronic properties of localized defects at surfaces and in the bulk

G Wachutka†, A Fleszar‡, F Máca§ and M Scheffler

Fritz-Haber-Institut der MPG, Faradayweg 4–6, D-1000 Berlin 33, Federal Republic of Germany

Received 10 October 1991

Abstract. We present a self-consistent Green-function method which enables parameter-free calculations of the charge density, the density of states, and related quantities in electronic systems where the three- or two-dimensional translational symmetry is broken by a perturbation which is localized in real space. In particular, the method is suited to study point defects in the interior of a metallic or semiconducting crystal or at a crystal surface. The self-consistent Green operator describes an infinitely extended system. The only restrictive assumption is that the self-consistent electronic structure of the *unperturbed* bulk material is well reproduced by a muffin-tin (pseudo) potential. In the *perturbed* region, however, no significant constraint is imposed either on the shape of the potential or on the charge density. While the basic ideas of our method have been published elsewhere [1], in this paper the practical aspects will be discussed. The numerical practicality and efficiency of a first implementation based on a Gaussian basis set is illustrated with reference to selected test calculations.

1. Introduction

In this article, we describe the practical aspects of a new method [1] based on the concepts of density-functional theory (DFT) [2, 3]. The method applies to a large class of electronic systems where the two- or three-dimensional periodicity is broken by a spatially localized perturbation. Typical examples include point defects (e.g. vacancies or impurities) in the bulk or at the surface of a crystal, or adsorbates (at low coverage) on a surface.

Our approach contrasts favourably with other so-called 'wavefunction methods' in several aspects. In the latter methods, one attacks the entire system directly in one single step by solving the system of Kohn–Sham equations in a self-consistent way. It is well known, however, that the solution of a Schrödinger-type equation implies a

† Permanent address: Swiss Federal Institute of Technology Zürich, Physical Electronics Laboratory, ETH Hoenggerberg, HPT, CH-8093 Zürich, Switzerland.

‡ Present address: Institute of Physics, University of Würzburg, Am Hubland, D-8700 Würzburg, Federal Republic of Germany.

§ Permanent address: Institute of Physics, Czechoslovak Academy of Sciences, Na Slovance 2, CS-18040 Prague 8, Czechoslovakia.

0953-8984/92/112831+14$04.50

boundary-value problem. As a consequence, the individual wavefunctions, the energy levels, and the density of states will not only depend on the spatial region of physical or chemical interest, but they may also be sensitive to the distant boundaries. The changes of the individual wavefunctions will usually reach far into the unperturbed material and, therefore, the Kohn–Sham equation needs to be solved within a range which extends largely outside the defect region. So even if supercomputing facilities are available, the computational effort can only be kept tractable by introducing strong simplifications of the original, infinitely extended geometry such as, e.g., cluster [4, 5] or slab or supercell [6–10] approximations.

An alternative way is provided by our Green-function method which takes advantage of the physical effect that *changes* in the Kohn–Sham effective potential $V_{\rm eff}(\boldsymbol{r})$ and in the electron density $n(\boldsymbol{r})$ are much more localized than the individual wavefunctions. In this approach, we follow a *two-step concept* and split the entire problem into two parts where each of them is far less complicated than the original one. This allows us to combine a proper physical description with computational practicality. The entire complex structure is decomposed into an infinitely extended, but tractable 'reference system' characterized by an effective single-particle potential $V^0(\boldsymbol{r})$ and a 'difference system' defined as the difference between the true (self-consistent) effective potential $V_{\rm eff}[n(\boldsymbol{r});\boldsymbol{r}]$ and $V^0(\boldsymbol{r})$ (cf figure 1)

$$\Delta V[n(\boldsymbol{r});\boldsymbol{r}] := V_{\rm eff}[n(\boldsymbol{r});\boldsymbol{r}] - V^0(\boldsymbol{r})\,. \tag{1}$$

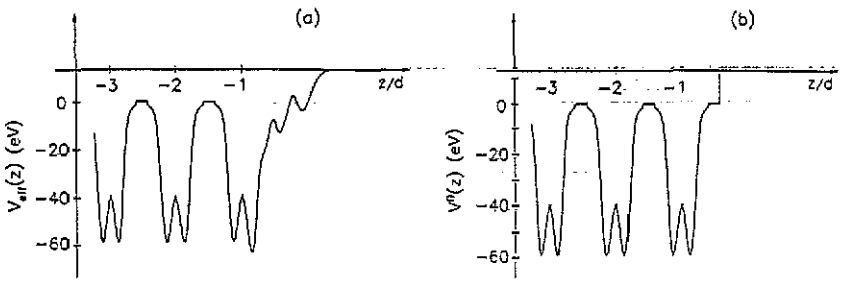

Figure 1. Schematic picture of the effective single-particle potential of the true system, i.e. an adatom chemisorbed at a surface (*a*) and of the reference system (*b*), i.e. a clean, semi-infinite substrate with a model surface potential. The substrate atoms are at positions $z/d = -1, -2, \ldots$.

For reasons which will become apparent below, the key idea in our approach is that the *change* of the potential, ΔV, as well as the *change* of the electronic charge density,

$$\Delta n(\boldsymbol{r}) = n(\boldsymbol{r}) - n^0(\boldsymbol{r}) \tag{2}$$

are supposed to be localized within a finite box A in real space, as soon as self-consistency is attained. $n^0(\boldsymbol{r})$ is the ground-state electron density of

$$\boldsymbol{H}^0 = -\frac{\hbar^2}{2m}\nabla^2 + V^0\,. \tag{3}$$

The complete set of electronic states of the reference system is represented by the 'reference Green operator'

$$\boldsymbol{G}^0(Z) := [Z - \boldsymbol{H}^0]^{-1} \tag{4}$$

and can be computed numerically at reasonable expense. $Z = E + i\eta$ is the complex single-particle energy ($\eta \geqslant 0$). The calculation of $\boldsymbol{G}^0(Z)$ along a properly chosen contour in the complex energy plane defines *step one* of our approach; practical methods for that are described elsewhere [11–14] and, hence, will not be discussed in this work.

In *step two*, the Green operator $\boldsymbol{G}(Z)$ of the true system (and the charge density related to it) is determined by solving Dyson's equation

$$\boldsymbol{G}(Z) = \boldsymbol{G}^0(Z) + \boldsymbol{G}^0(Z)\Delta V \boldsymbol{G}(Z) \tag{5}$$

in a self-consistent way. In contrast to the so-called 'matrix Green function' methods [15–18] which, after introducing a set of appropriate basis functions, make use of equations (3)–(5) in matrix representation, we treat the relations (3)–(5) as operator equations. Writing the operator $\boldsymbol{G}(Z)$ as

$$\boldsymbol{G}(Z) = \boldsymbol{G}^0(Z) + \Delta\boldsymbol{G}(Z) \tag{6}$$

reveals that only the difference operator $\Delta\boldsymbol{G}(Z)$ (and the difference electron charge density $\Delta n(\boldsymbol{r})$ related to it) actually needs to be calculated in step two. The advantage of this scheme is that, by construction, $\boldsymbol{G}(Z)$ satisfies the correct boundary conditions of the infinite system (through $\boldsymbol{G}^0(Z)$) and allows for full flexibility in the perturbed region (by virtue of $\Delta\boldsymbol{G}(Z)$).

In section 2 of this paper it is shown that it is only the projection of $\Delta\boldsymbol{G}(Z)$ onto the box A which has to be evaluated numerically and, therefore, only this quantity needs to be well approximated by a finite number of basis functions. In section 3 we summarize some important practical and technical aspects of our method. In section 4 some test calculations are discussed. These tests have been performed using examples which are rather difficult for the method, because we like to show the advantages as well as the limitations of our approach. In section 5 we summarize our results. Throughout this paper operators are noted by bold italic face symbols and the corresponding matrices are typeset in gothic.

2. Basic theory

Since the basic features of our method have been discussed elsewhere [1], we focus here on those aspects of the theory which are relevant for the computational practice.

The self-consistency loop is schematically illustrated in the flow diagram in figure 2.

We start with a guessed difference electron distribution Δn and thus obtain an initial value of the electron density $n(\boldsymbol{r}) = n^0(\boldsymbol{r}) + \Delta n(\boldsymbol{r})$. From this, the Hartree contribution

$$\Delta V_{\mathrm{H}}[\Delta n; \boldsymbol{r}] = e^2 \int_A \frac{\Delta n(\boldsymbol{r}')}{|\boldsymbol{r} - \boldsymbol{r}'|} \mathrm{d}\boldsymbol{r}' \tag{7}$$

where e is the elementary charge, and the exchange-correlation contribution

$$\Delta V_{\mathrm{xc}}[\Delta n; \boldsymbol{r}] = V_{\mathrm{xc}}[n^0(\boldsymbol{r}) + \Delta n(\boldsymbol{r}); \boldsymbol{r}] - V_{\mathrm{xc}}[n^0(\boldsymbol{r}); \boldsymbol{r}] \tag{8}$$

are computed to update ΔV according to the relation

$$\Delta V = \Delta V_{\mathrm{ion}} + \Delta V_{\mathrm{H}}[\Delta n] + \Delta V_{\mathrm{xc}}[\Delta n] + \Delta V_{\mathrm{sc}}^0 . \tag{9}$$

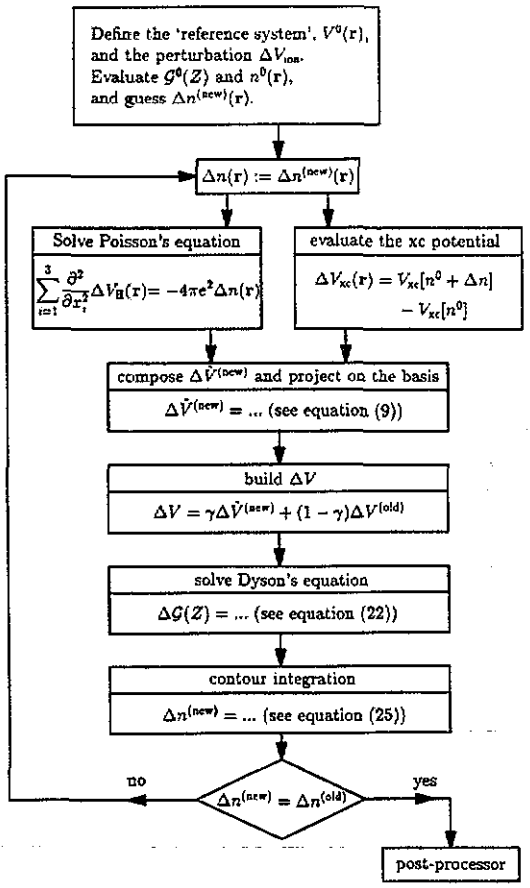

Figure 2. Flow diagram of the self-consistency loop.

Here $\Delta V_{\rm ion}$ denotes the (possibly non-local) unscreened ionic defect potential; in practice, norm-conserving *ab initio* pseudo potentials [19, 20] are favourably used. We also add in equation (9) a term $\Delta V_{\rm sc}^0$ which takes into account the fact that the reference system, defined by V^0, need not necessarily be a self-consistent potential. If V^0 and n^0 are self-consistent, $\Delta V_{\rm sc}^0$ is zero. If, however, V^0 is not fully self-consistent (e.g. because a model surface potential or a muffin-tin approximation is used), we obtain

$$\Delta V_{\rm sc}^0 = V_{\rm ion}^0 + V_{\rm H}[n^0] + V_{\rm xc}[n^0] - V^0 . \tag{10}$$

$V_{\rm ion}^0$ are the ionic (pseudo) potentials underlying the reference-system potential V^0. Including $\Delta V_{\rm sc}^0$ in (9) implies that the approximations done at the first level of the calculation will be corrected at the second level (see below). Obviously, V^0 should be chosen such that $\Delta V_{\rm sc}^0$ is localized. This implies that any choice of V^0 should be close to a self-consistent potential. This appears to be a significant constraint on V^0. However, we note that the remaining freedom allows us to improve the efficiency and numerical accuracy to evaluate $\boldsymbol{G}^0(Z)$ significantly. Let us now exploit the localization of ΔV and of Δn. Since the change of the electron density is confined to the rather small spatial region A, it can be calculated by

$$\Delta n(r) = -\frac{2}{\pi} \mathrm{Im} \int_C \langle r \mid \boldsymbol{P} \Delta \boldsymbol{G}(Z) \boldsymbol{P} \mid r \rangle \mathrm{d}Z . \tag{11}$$

Here $\boldsymbol{P}$ denotes the projection onto the region A in real space, and C is a contour in the upper half of the complex energy plane joining $-\infty$ with E_F, the Fermi energy of the unperturbed (reference) system. Therefore, it suffices to solve Dyson's equation (5) together with (6) only for the quantity $\boldsymbol{P}\Delta\boldsymbol{G}(Z)\boldsymbol{P}$ by making use of

$$\boldsymbol{P}\Delta\boldsymbol{G}(Z)\boldsymbol{P} = \boldsymbol{P}\boldsymbol{G}^0(Z)\boldsymbol{P}\Delta V\boldsymbol{P}(\boldsymbol{P}\boldsymbol{G}^0(Z)\boldsymbol{P} + \boldsymbol{P}\Delta\boldsymbol{G}(Z)\boldsymbol{P}). \tag{12}$$

This equation immediately follows from (5) if only the relation

$$\boldsymbol{P}\Delta V\boldsymbol{P} = \Delta V \tag{13}$$

is valid (note that $\boldsymbol{P}\boldsymbol{P} = \boldsymbol{P}$). As in typical applications the perturbation potential ΔV_{ion} is efficiently screened at larger distances from the centre of the perturbation, because it is cancelled by ΔV_{H}, (13) can indeed be satisfied at a high level of numerical accuracy. We note that perturbations in bulk semiconductors (see e.g. [21]) are typically screened within a distance of about 1–2 bond lengths. This even holds within an acceptable approximation for charged defects. At metal surfaces the screening may be less efficient: for ionically bound adsorbates the perturbation potential falls off by a power law, thus much slower than an exponential. Based on our experience we tend to conclude that this power-law tail of the potential (often called Friedel oscillations) has a rather small prefactor for typical metals (e.g. Al or Pd). Therefore, neglecting this long-range tail of the potential-perturbation will not affect the results perceptibly. For high r_s-value jellium-like metals, i.e. for $r_s \gtrsim 4$, these Friedel oscillations are expected to be more important. In this case a better basis set covering a larger region in real space may be needed.

After solving (12), the 'new' difference charge distribution obtained from (11) is compared with the initial ('old') one. If the difference is found to be smaller than the desired tolerance, Δn is accepted as the self-consistent result and, together with $\Delta\boldsymbol{G}(Z)$ and ΔV, passed to the post-processor level of the calculation. Otherwise the self-consistency cycle is repeated with Δn replaced by $\Delta n^{(\text{new})}$.

The post-processor serves to evaluate certain functions or functionals of $\Delta\boldsymbol{G}(Z)$ or ΔV. As a matter of fact, $\Delta\boldsymbol{G}(Z)$ (or $\boldsymbol{G}(Z)$) are central quantities which completely characterize the electronic properties of the system under consideration. Hence any physical observable of interest can be extracted from it, such as, e.g., the change of the electron density (see equation (11)), the change of the total density of states,

$$\Delta N(E) = -\frac{2}{\pi}\frac{\mathrm{d}}{\mathrm{d}E}\lim_{\eta\to+0}\operatorname{Im}\ln\det\left(1 - \boldsymbol{G}^0(E+\mathrm{i}\eta)\Delta V\right) \tag{14}$$

the local density of states,

$$N(E,\boldsymbol{r}) = -\frac{2}{\pi}\lim_{\eta\to+0}\operatorname{Im}\langle\boldsymbol{r}\mid\boldsymbol{G}(E+\mathrm{i}\eta)\mid\boldsymbol{r}\rangle \tag{15}$$

the density matrix,

$$n(\boldsymbol{r},\boldsymbol{r}') = -\frac{2}{\pi}\operatorname{Im}\int_C\langle\boldsymbol{r}\mid\boldsymbol{G}(Z)\mid\boldsymbol{r}'\rangle\mathrm{d}Z \tag{16}$$

or dipole moments, change of the work function etc. In particular, $\boldsymbol{G}(Z)$ contains all of the information required for total energy and force calculations [2, 3, 16, 18, 22, 23].

3. Practical realization

In this section we describe some technical details of the self-consistency scheme. The projector $\boldsymbol{P}$ onto the box A is approximated as follows: we choose a set of localized, linearly independent functions

$$\langle \boldsymbol{r} \mid g_I \rangle = g_I(\boldsymbol{r}) \qquad I = 1, \ldots, N \tag{17}$$

which 'cover' A in the sense that the projector

$$\hat{\boldsymbol{P}} := \sum_{I,J} |g_I\rangle \left(\mathcal{S}^{-1}\right)_{IJ} \langle g_J| \tag{18}$$

(with $S_{IJ} := \langle g_I | g_J \rangle$ being the overlap matrix) is an acceptable approximation of $\boldsymbol{P}$. Here 'acceptable' means that

$$\mathrm{Im} \int_C \langle \boldsymbol{r} \mid \Delta \boldsymbol{G}(Z) \mid \boldsymbol{r} \rangle \mathrm{d}Z \approx \mathrm{Im} \int_C \sum_{I,J} g_I(\boldsymbol{r}) \Delta G_{IJ}(Z) g_J^*(\boldsymbol{r}) \mathrm{d}Z \tag{19}$$

holds with sufficient accuracy in region A. The matrix elements ΔG_{IJ} are defined by

$$\Delta G_{IJ}(Z) := \sum_{K,L} (\mathcal{S}^{-1})_{IK} \langle g_K \mid \Delta \boldsymbol{G}(Z) \mid g_L \rangle (\mathcal{S}^{-1})_{LJ} \,. \tag{20}$$

We should mention that in our previous paper [1] we omitted the factors $\mathcal{S}^{-1}$ for the sake of a simple notation. This is equivalent to assuming an orthonormal basis set. In the present implementation of our method, the g_I are Gaussian orbitals

$$g_{\alpha l m \boldsymbol{R}}(\boldsymbol{r}) := \mathrm{e}^{-\alpha |\boldsymbol{r}-\boldsymbol{R}|^2} |\boldsymbol{r} - \boldsymbol{R}|^l Y_{lm}(\boldsymbol{r} - \boldsymbol{R}) \tag{21}$$

placed at appropriately chosen positions $\boldsymbol{R} \in A$ and falling off with decay constants $\alpha > 0$. Y_{lm} denote the spherical harmonics; hence, $|\boldsymbol{r} - \boldsymbol{R}|^l Y_{lm}(\boldsymbol{r} - \boldsymbol{R})$ are harmonic polynomials centred at R. The reason for choosing Gaussians as the basis set is primarily that they exhibit convenient integration and expansion properties, so that in the evaluation of matrix elements a considerable part of computational work can be done analytically. After the Gaussian basis has been introduced, the present method is essentially identical to the defect-Green-function method of Scheffler *et al* [21, 24, 22]. The only differences are that, in the present version, instead of orthonormalizing the Gaussian basis we carry the $\mathcal{S}$ matrix along, and that we avoid exploiting group theory. Our approach shows some formal similarities with the defect-Green-function methods of Bernholc *et al* [25], Baraff and Schlüter [26], and Braspenning *et al* ([27] and references therein). In the practical realization, however, there are substantial differences which give the present method all the flexibility required for handling low-*symmetry defects and in particular, defects at surfaces and interfaces.*

With $\hat{\boldsymbol{P}}$ substituted for $\boldsymbol{P}$ in equation (12), we arrive at a discretized version (= Gauss orbital representation) of Dyson's equation which can be solved algebraically for the unknown quantity $\Delta \mathcal{G}(Z)$

$$\Delta \mathcal{G}(Z) = \left[(1 - \mathcal{G}^0(Z) \mathcal{S}^{-1} \Delta \mathcal{V} \mathcal{S}^{-1})^{-1} - 1 \right] \mathcal{G}^0(Z) \,. \tag{22}$$

Here, all matrices are understood with respect to the Gaussian orbitals, which implies the occurrence of the inverse overlap matrix, $\mathcal{S}^{-1}$, due to the non-orthogonality of the basis functions $g_{\alpha lmR}$. For the practical evaluation of $\langle g_I|\mathbf{G}^0(Z)|g_J\rangle$, first the $\boldsymbol{k}_\parallel$-resolved angular momentum representation of $\boldsymbol{G}^0(Z)$, as it is obtained from the layer KKR-method [12],

$$\langle \boldsymbol{R}_i + \boldsymbol{r} \mid \boldsymbol{G}^0(Z,\boldsymbol{k}_\parallel) \mid \boldsymbol{R}_j + \boldsymbol{r}'\rangle = \sum_{lml'm'} G^0_{ilmjl'm'}(r,r')Y_{lm}(\hat{r})Y^*_{l'm'}(\hat{r}') \tag{23}$$

is semi-analytically transformed into an expansion in terms of the orbitals $g_{\alpha lmR}$. The details of the somewhat involved algebra are described in [14]. Then a numerical integration over the two-dimensional Brillouin zone, BZ_2, is performed by means of an efficient and accurate Gaussian-type quadrature formula [28] yielding

$$\langle g_I \mid \boldsymbol{G}^0(Z) \mid g_J\rangle = \frac{F}{(2\pi)^2}\int_{\mathrm{BZ}_2}\langle g_I \mid \boldsymbol{G}^0\left(Z,\boldsymbol{k}_\parallel\right) \mid g_J\rangle \mathrm{d}^2\boldsymbol{k}_\parallel \tag{24}$$

where F is the area of the two-dimensional unit cell. We note that along the path segments C_1 and C_2 (see figure 3) the $\boldsymbol{k}_\parallel$ integration converges quite rapidly. Special care is necessary, of course, at the Fermi surface, i.e. for $Z \to E_\mathrm{F}$.

Typical linear dimensions of the matrices found in the discretized equations are $N = 50$–350 (= number of Gaussians); for instance, a 9-centre, 3-decay, s, p, d-basis results in $N = 9\times3\times9 = 243$. The computational expense required for evaluating (22) numerically comprises four full matrix multiplications and one full matrix inversion per energy value. Since the numerical integration of (11) typically involves about 50–100 sample points, the use of vectorization or parallelization techniques is obviously advantageous. One should note that the time-consuming calculation of $\mathcal{G}^0(Z)$ has to be done only once (in step one of our scheme) on a pre-selected sequence of energy sample points $Z_k \in \mathbb{C}$ which are determined by the quadrature rule used in the subsequently discussed complex energy integration.

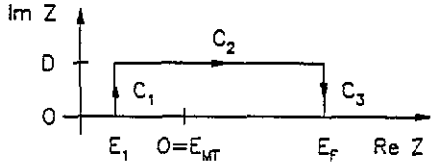

Figure 3. Energy contour used for complex charge density integration. D denotes the imaginary part which is typically chosen as 2 eV. E_1 will be sufficiently far below the bottom of the band.

The change of the charge density $\Delta n(\boldsymbol{r})$ is most efficiently obtained by evaluating equation (11) by means of the numerical integration

$$\Delta n(\boldsymbol{r}) = \mathrm{Im}\sum_{I,J}\left(\mathcal{S}^{-1}\Delta\mathcal{C}\mathcal{S}^{-1}\right)_{IJ} g_I(\boldsymbol{r})g^*_J(\boldsymbol{r}) \tag{25}$$

where

$$\Delta\mathcal{C} := -\frac{2}{\pi}\int_C \Delta\mathcal{G}(Z)\mathrm{d}Z\,. \tag{26}$$

Because the Green-function operator $G^0(Z)$ is evaluated very accurately for its real and its imaginary part (see [12] and [14]) our method allows for the treatment of nearly-free electron metals as well as for transition metals. In practice, the integration path C reaching from $-\infty$ to E_F is realized as a rectangular contour, $C = C_1 + C_2 + C_3$ in the upper half of the complex energy plane as shown in figure 3. This is advantageous because typically the integrand in equation (11) shows rapid variations along the real energy axis which are the more broadened and smoothened, the more the imaginary part of the energy grows. Consequently, as the distance D between the contour and the real axis increases, the sample points used in the quadrature rule can be chosen less dense on path C_2. The total number of sample points required for a certain numerical accuracy will attain a minimum for a certain distance D. In view of the computational expense for solving (22), it is obvious that minimizing the number of sample points is worthwhile. Empirical values for the optimal choice of D are about 1–2 eV, in accordance with other investigations [17, 18, 22, 29].

Having $\Delta n(\boldsymbol{r})$ obtained through $\Delta\mathcal{C}$, we need to recalculate the charge-dependent contributions to ΔV. For this purpose, a three-dimensional equidistant discretization grid $\{\boldsymbol{r}_j\}_{j=1,\ldots,\mathrm{NP}}$ is defined within the box A (a typical number of points is NP $\simeq 10^4$), and Δn is evaluated on the grid points $\boldsymbol{r}_j$. The point values $\Delta V_{\mathrm{xc}}(\boldsymbol{r}_j)$ are now easily obtained by equation (8), while the Hartree contribution $\Delta V_{\mathrm{H}}(\boldsymbol{r}_j)$ is computed by solving Poisson's equation

$$\sum_{i=1}^{3} \frac{\partial^2}{\partial x_i^2} (\Delta V_{\mathrm{H}}) = -4\pi e^2 \Delta n \tag{27}$$

by means of Fast Fourier Transform (FFT) techniques [24, 30]. Then the matrix elements of the electron density-dependent contributions to ΔV with respect to the Gaussian orbitals are calculated by equidistant numerical integration over A

$$\langle g_I \mid \Delta V_{\mathrm{H}} + \Delta V_{\mathrm{xc}} \mid g_J \rangle \approx \sum_{j=1}^{\mathrm{NP}} g_I^*(\boldsymbol{r}_j)\left[\Delta V_{\mathrm{H}}(\boldsymbol{r}_j) + \Delta V_{\mathrm{xc}}(\boldsymbol{r}_j)\right] g_J(\boldsymbol{r}_j)\Delta v \tag{28}$$

where Δv denotes the volume of the box A divided by NP. Since all these operations tend to become expensive in terms of CPU time and memory, a careful choice of the grid spacing is most useful. The requirements are to ensure sufficient spatial resolution of $\Delta n(\boldsymbol{r})$ for the FFT step as well as to keep the integration error of equation (28) within tolerable bounds. One should note that the matrix elements of the non-local part of ΔV, i.e. of ΔV_{ion} (cf (9)), have to be computed only once when initializing the entries for the self-consistency loop.

To avoid oscillations or possible divergence of the self-consistency cycles, it is necessary to damp the iteration procedure. From a mathematical point of view, we deal with a fixed-point problem where the underlying iteration mapping has to be controlled by a relaxation parameter γ in such a way that Banach's fixed-point theorem applies [31]. In our present approach we achieve this by 'potential mixing': only a fractional part of the updated potential $\Delta\tilde{V}^{(\mathrm{new})}$ (as obtained from the evaluation of (9)) is actually used for the computation of $\Delta\mathcal{G}(Z)$ in the subsequent cycle:

$$\Delta V = \gamma \Delta\tilde{V}^{(\mathrm{new})} + (1-\gamma)\,\Delta V^{(\mathrm{old})}\,. \tag{29}$$

For $\gamma = 0$, no improvement of ΔV is made, but the iteration is absolutely stable. Choosing a small $\gamma > 0$ results in a slight improvement of ΔV, with the iteration being

still stable; however, the rate of convergence will be slow. So it is desirable to increase the mixing weight γ in a self-adaptive way in order to accelerate the convergence, but without overstepping the point where the iteration process starts oscillating or diverging. Hence, the optimal choice of the relaxation parameter γ consists in finding a condition under which the rate of convergence attains its maximum value. This idea can be expressed quantitatively as follows: we define the 'residual' of the jth iteration step as

$$\rho_j(\gamma) := \|\Delta\tilde{V}_j^{(\mathrm{new})} - \Delta V_j^{(\mathrm{old})}\| \tag{30}$$

where $\Delta V_j^{(\mathrm{old})}$ has been used as input for step j (with mixing weight γ), while $\Delta\tilde{V}_j^{(\mathrm{new})}$ is the updated but *undamped* difference potential *after* step j.$\|\ldots\|$ may be any norm, but in the present context it is convenient to use the L_2-operator norm which is easily obtained by

$$\|\Delta V\|_2 = \sqrt{\mathrm{tr}\left((\Delta \boldsymbol{V}\boldsymbol{S}^{-1})^2\right)}\,. \tag{31}$$

The rate of convergence is then given by

$$w(\gamma) := -\frac{\rho_{j+1}(\gamma) - \rho_j(\gamma)}{(j+1) - j} = \rho_j(\gamma) - \rho_{j+1}(\gamma)\,. \tag{32}$$

Unfortunately, the exact value of $w(\gamma)$ can be determined only *a posteriori*. However, from the general properties of relaxation methods [32], the qualitative behaviour of the curve $w(\gamma)$ is known (figure 4) and, therefore, can be exploited: at $\gamma = 0$, we have the trivial case $w(\gamma) = 0$. Then, $w(\gamma)$ will monotonously grow until the maximum value is reached at $\gamma = \gamma_{\mathrm{opt}}$. Subsequently, $w(\gamma)$ falls off very quickly and changes sign, indicating that the iteration becomes divergent here. Thus, for obtaining an estimate of γ_{opt}, we monitor the convergence history for some distinct trial values $\gamma_1 < \gamma_2 < \gamma_3 \cdots$ and fit a parabola to the recorded values of $w(\gamma_k)$; the maximum of the parabola yields an approximate value of γ_{opt}, which will be used for the subsequent iteration step. Repeating this procedure at any step, the approximate value of γ_{opt} is continuously updated and so an optimal control algorithm for the mixing weight γ is obtained. Test calculations (figure 5) have shown that by this method a considerable convergence acceleration can be achieved, and that the automatic control is stable enough to recover even in the case of overstepping the optimum γ_{opt} (figure 5(b)).

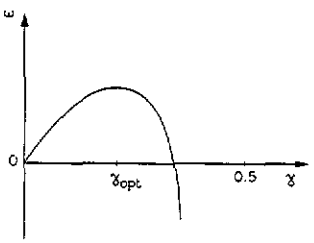

Figure 4. Convergence rate of the self-consistency iteration versus the damping parameter γ (schematic).

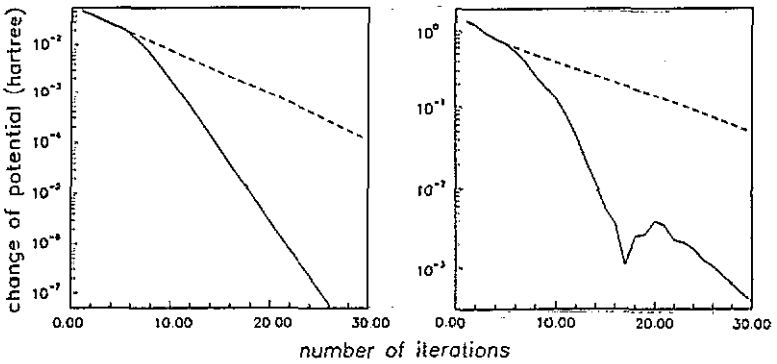

Figure 5. Convergence history of the self-consistency loop. The full curves are the result of the described optimization procedure (see equations (29)–(32)). The broken curves follow, when the damping parameter γ is kept at a fixed value. Left: hydrogen atom in empty lattice; right: vacancy in bulk aluminium.

4. Test calculations

Several tests of the practicality and numerical accuracy of our self-consistent Green-function method have been performed. For example, we calculated the spectrum and the wavefunctions of a hydrogen atom embedded in an empty lattice and equipped with a partially filled 1s shell. As another test, we studied a vacancy in bulk aluminium. These test examples were chosen because in these cases results from independent and alternative methods were available for comparison.

To estimate the absolute accuracy of the contour integration, we integrated the change of the electron density over the enclosing box A and compared this value, Q_{int}, with the integrated change of the total density of states,

$$Q_{\mathrm{dos}} := \int_{-\infty}^{E_{\mathrm{F}}} \Delta N(E)\mathrm{d}E = \frac{2}{\pi}\left[\delta(E_{\mathrm{F}}) - \delta(-\infty)\right] \tag{33}$$

where

$$\delta(E) := -\lim_{\eta \to +0} \mathrm{Im} \ln \det\left(1 - \mathcal{G}^0(E + \mathrm{i}\eta)\mathcal{S}^{-1}\Delta\mathcal{V}\mathcal{S}^{-1}\right) \tag{34}$$

is the generalized scattering phase shift [33]. Without basis-set effects and quadrature error, Q_{int} and Q_{dos} have to be equal. Moreover, if perfect charge screening is attained, they exactly compensate the change of ionic charge, Q_{ion}, which is given by the unscreened perturbation potential, ΔV_{ion}. In our tests the deviations of Q_{int} and Q_{dos} from $-Q_{\mathrm{ion}}$ proved to be within tolerable bounds ($\leqslant 2\%$).

Figure 6 shows a family of curves representing the ground-state energy level of the hydrogen atom with partially occupied 1s state. The full curve shows the correct relation as obtained by integration of the radial atomic Kohn–Sham equation. The other curves show results of Green-function calculations using an empty FCC lattice and a lattice constant of aluminium. The discrepancies are not astonishing because an empty-lattice test is a tough challenge to a method where the Green function is calculated from scattering theory and numerical $k_{\parallel}$-integration so that we are certainly close or beyond the limits of its capability. It should also be noted that we

have an extremely strong perturbation in this case, because $n^0(r) = 0$ and hence $\Delta n(r) = n(r)$. Figure 7 reveals the additional complication of approximating the hydrogen e^2/r potential by a tensor product of Gaussians. Nevertheless, figure 6 clearly demonstrates that, with an appropriate choice of the basis set, the true energy level can be approached either from above or below. It should be mentioned here that our Green-function method does not obey a variational principle for the single-particle energies; hence a minimum property for energy levels cannot be expected. For total energies, the variational principle of $E^{\text{total}}[n]$ can, however, be applied. The proper selection of the decays α and the orbital sites $\boldsymbol{R}$ in the *ansatz* (21) thus turns out to be the difficult point in our method. A rigorous approach to measure the quality of the basis would necessitate the use of a physically meaningful variational expression [34] such as, for example, the total energy. Our present problem is illustrated in figure 8 which shows the squared 1s wavefunction as obtained with a proper and with a poor basis set. The differences between the exact result and the Green-function calculation look very large. It should be noted, however, that the small r region does not play an important role, because of the small volume element $r^2 dr$.

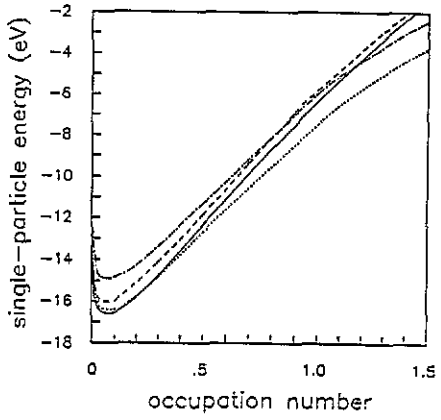

Figure 6. DFT–LDA [29] calculations for the single-particle energy of a hydrogen atom as a function of the 1s level occupation. The full curve shows the correct result. The other curves show results of Green-function calculations: monocentre s-basis with decays 0.1, 0.9, 1.6 bohr^{-2} (chain curve), monocentre s-basis with decays 0.3, 0.6, 1.2 bohr^{-2} (dotted curve), 13-centre s,p,d-basis with decays 0.1, 0.5, 1.0 bohr^{-2} (broken curve).

As another test example, where screening is crucial, we treated the vacancy in bulk aluminium. Here the defect charge (the removed Al nucleus) is screened by the crystal electrons surrounding the vacancy. We compared the self-consistent potential and charge distribution resulting from our Green-function method with self-consistent supercell calculations based on the same ionic bulk potential [19]. In figure 9 we show results of a self-consistent Al bulk calculation, as well as of calculations for an aluminium vacancy. For all calculations norm-conserving pseudopotentials are used. Figure 9(a) shows the bulk electron density and figures 9(c) and 9(d) show charge density *differences* of vacancy supercell calculations. The basis set for these three calculations consists of plane waves with a kinetic energy up to 12 Ryd. For the crystal we use a one-atom cell and evaluate the $\boldsymbol{k}$ integrals with 146 special points. Figure 9(c) corresponds to an 8-atom supercell and using 19 special $\boldsymbol{k}$ points, and figure 9(d)

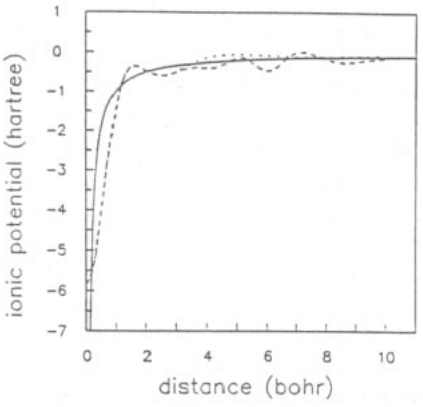

Figure 7. Exact $-e^2/r$ potential (full curve) and its approximation by a 13-centre s, p, d-basis with decays 0.1, 0.5, 1.0 bohr^{-2} along the [100] direction (dotted curve), and along the [110] direction (broken curve).

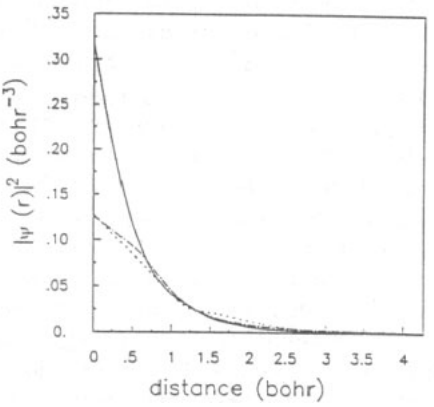

Figure 8. Squared 1s wavefunction of a hydrogen atom, $V_{\text{eff}}(r) = -e^2/r$: exact result (full curve); monocentre basis with decays 0.1, 0.9, 1.6 bohr^{-2} (chain curve); monocentre basis with decays 0.3, 0.6, 1.2 bohr^{-2} (dotted curve).

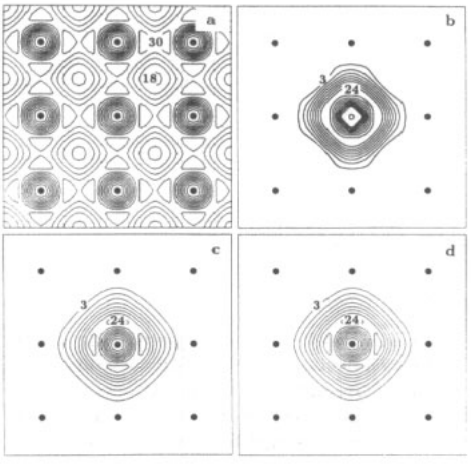

Figure 9. (*a*) Self-consistent charge density of an Al crystal along the (100)-plane. (*b*) Screening charge density around a vacancy in bulk aluminium as obtained with our Green-function method (13-centre s, p, d-basis, decays = 0.3, 0.5, 1.0 bohr^{-2}). (*c*) Same as (*b*) but calculated with a supercell approach with 8 atoms per cell. (*d*) Same as (*c*) but with 27 atoms per cell. Units are 10^{-3} e bohr^{-3}. Atoms are indicated by full circles.

corresponds to a 27-atom super cell with 6 special k points. Figure 9(*b*) shows the result of a Green-function calculation using a 13-centre basis. In the two supercell calculations (figures 9(*c*) and 9(*d*)) the electron density is practically identical, which reflects the earlier stated point that screening of perturbations in metals is very efficient and that long-range Friedel oscillations are not important for small-r_s metals. The Green-function method gives slightly different results. These differences arise because the Green-function method uses a different basis set (Gaussians centred at 13 sites

amounting to 351 basis functions). For a nearly-free-electron metal this is apparently not as flexible as the plane-wave basis (for the 8-atom cell there are $12 \times 48 \times 610 = 351\,360$ basis functions). The differences between figure 9(*b*) and figures 9(*c*), (*d*) are, however, not important, i.e. the spatial extension and shape of $\Delta n(\boldsymbol{r})$ obtained by the Green-function calculation and by the super cell calculation are in essence identical. The difference in the 24×10^{-3} e bohr^{-3} line, i.e. the fact that we obtain two closed rings of 24×10^{-3} e bohr^{-3} in the Green-function approach but four triangle-shaped local maxima in the two supercell calculations, is not significant.

5. Summary

In this article we discussed some practical aspects of a new self-consistent Green-function method which allows first-principles calculations of the electronic properties of infinite or semi-infinite systems where a localized perturbation destroys the two- or three-dimensional periodicity. Provided the electronic structure of the *unperturbed* material is well represented by a muffin-tin (pseudo) potential, there is no significant constraint on the shape of the potential or the electron density in the vicinity of the perturbation. The asymptotic behaviour far away from the perturbation correctly reflects the system to be investigated.

The individual steps of the self-consistency loop are explained. In particular, computationally efficient discretization schemes for Dyson's equation and Poisson's equation are described and the problem of optimal energy integration is treated. Furthermore, an algorithm for convergence acceleration is presented which is based on the optimal control of potential mixing.

Test calculations have been made to examine the numerical accuracy of our method. They demonstrate its computational practicality and efficiency, but also reveal the implications caused by the definition of the basis set used in the present implementation.

Acknowledgments

The authors are grateful to K Kambe, Ch Droste, G Barzel, and J Bormet for stimulating discussions. We thank V Schmid for help with the calculations shown in figures 6 and 8.

References

[1] Scheffler M, Droste Ch, Fleszar A, Máca F, Wachutka G and Barzel G 1991 *Physica* B **172** 143
[2] Hohenberg P and Kohn W 1964 *Phys. Rev.* B **136** 864
[3] Kohn W and Sham L J 1965 *Phys. Rev.* A **140** 1133
[4] Müller J 1986 *Surf. Sci.* **178** 589
[5] Hermann K, Bagus P S and Nelin C J 1987 *Phys. Rev.* B **35** 9467; 1987 *Appl. Phys.* A **44** 63
[6] Krakauer H, Posternak M and Freeman A J 1979 *Phys. Rev.* B **19** 1706
Weinert M, Wimmer E and Freeman A J 1982 *Phys. Rev.* B **26** 4571
[7] Cohen M L 1985 *Highlights of Condensed-Matter Theory* ed F Bassani, F Fumi and M P Tosi (Amsterdam: North-Holland) p 16
[8] Bohnen K P and Ho K M 1990 *Vacuum* **41** 416
[9] Manghi F, Sole R Del, Selloni A and Molinari E 1990 *Phys. Rev.* B **41** 9935

[10] Scheffler M and Dabrowski J 1988 *Phil. Mag.* A **58** 107
[11] Kambe K and Scheffler M 1979 *Surf. Sci.* **89** 262
[12] Máca F and Scheffler M 1985 *Comput. Phys. Commun.* **38** 403; 1987 *Comput. Phys. Commun.* **47** 349; 1988 *Comput. Phys. Commun.* **51** 381
[13] Wachutka G 1988 *Ann. Phys., NY* **187** 269&314
[14] Droste Ch 1990 *PhD thesis* Technische Universität, Berlin
[15] Williams A R, Feibelmann P J and Lang N D 1982 *Phys. Rev.* B **26** 5433
[16] Feibelmann P J 1987 *Phys. Rev.* B **35** 2626
[17] Krüger P and Pollmann J 1988 *Phys. Rev.* B **38** 10578
[18] Beeler F, Andersen O K and Scheffler M 1990 *Phys. Rev.* B **41** 1603
[19] Hamann D R, Schlüter M and Chiang G 1979 *Phys. Rev. Lett.* **43** 1494
[20] Kerker G 1980 *J. Phys. C: Solid State Phys.* **13** L189
[21] Scheffler M 1982 *Adv. Solid State Phys.* **22** 115; 1987 *Physica* B **146** 176
[22] Scheffler M, Vigneron J P and Bachelet G B 1982 *Phys. Rev. Lett.* **49** 1765; 1985 *Phys. Rev.* B **31** 6541
[23] Baraff G A and Schlüter M 1983 *Phys. Rev.* B **28** 2296
[24] Scheffler M, Bernholc J, Lipari N O and Pantelides S T 1984 *Phys. Rev.* B **29** 3269
[25] Bernholc J, Lipari N O and Pantelides S T 1978 *Phys. Rev. Lett.* **41**, 895; 1980 *Phys. Rev.* B **21** 3545
[26] Baraff G A and Schlüter M 1978 *Phys. Rev. Lett.* **41** 892; 1979 *Phys. Rev.* B **19** 4965
[27] Braspenning P J, Zeller R, Lodder A and Dederichs P H 1984 *Phys. Rev.* B **29** 703
[28] Cowper G R 1973 *Int. J. Num. Meth. Eng.* **7** 405
[29] A discussion of the advantages and drawbacks of other integration paths may be found in: Zeller R, Deutz J and Dederichs P H 1982 *Solid State Commun.* **44** 993
[30] Hockney R W 1970 *Methods in Computational Physics* vol 9 ed B Alder, S Fernbach and M Rotenberg (New York: Academic) p 135
[31] Edwards R E 1965 *Functional Analysis* (New York: Holt, Rinehart and Winston) ch 3
[32] Varga R S 1962 *Matrix Iterative Analysis* (Englewood Cliffs,NJ: Prentice-Hall)
[33] Callaway J 1964 *J. Math. Phys.* **5** 783
[34] Klink W H and Payne G L 1976 *J. Comput. Phys.* **21** 208